Nuclear Inst. and Methods in Physics Research, A 910 (2018) 15–21

Contents lists available at ScienceDirect

Nuclear Inst. and Methods in Physics Research, A

journal homepage: www.elsevier.com/locate/nima

Characterisation of the fused silica surface quality with a β-source

A. Natochii [a,b,c,*], L. Burmistrov [a], F. Addesa [d], O. Bezshyyko [b], D. Breton [a], V. Chaumat [a], G. Cavoto [d], S. Dubos [a], Y. Gavrikov [e], F. Iacoangeli [d], J. Maalmi Di Bello [a], S. Montesano [c], V. Puill [a], R. Rossi [c], W. Scandale [c], A. Stocchi [a]

[a] Laboratoire de l'Accélérateur Linéaire (LAL), Université Paris-Sud 11, Centre Scientifique d'Orsay, B.P. 34, Orsay Cedex, F-91898, France
[b] Taras Shevchenko National University of Kyiv (TSNUK), 60 Volodymyrska Street, City of Kyiv, 01033, Ukraine
[c] CERN, European Organization for Nuclear Research, CH 1211, Geneva 23, Switzerland
[d] INFN Sezione di Roma, Piazzale Aldo Moro 2, 00185 Rome, Italy
[e] Petersburg Nuclear Physics Institute in National Research Centre "Kurchatov Institute", 188300 Gatchina, Russia

ARTICLE INFO

Keywords:
Cherenkov radiation
Monte-carlo simulation
Fused silica quality

ABSTRACT

A method to characterise the quality of a fused silica surface using a β-source is presented. Two fused silica bars ($5 \times 10 \times 400$ mm^3) were fabricated for the Cherenkov detector for proton Flux Measurement installed at vacuum chamber of the Super Proton Synchrotron at CERN. The resolution of such device is defined by the collection efficiency of the Cherenkov light, which is produced by relativistic charged particles in the fused silica. Thus, the surface quality of the radiator should be as good as possible to avoid light losses. The method is based on the scanning of the radiator surface with a ^{90}Sr radioactive source and measurements of the Cherenkov light rate, detected by a PMT attached to the quartz bars. The data have been compared with a Monte-Carlo simulation, providing an estimation of the radiator's probability of the total internal reflection and inefficient area at the edges of the bars.

1. Introduction

Usually, to characterise the surface quality of fused silica, optical interferometers [1] or the method based on the scalar scattering theory [2,3] can be used. In this paper we propose a new method for surface and edge quality characterisation of fused silica with a β-source. We consider two dominant effects that influence the collection efficiency of the light produced in the radiator, namely the surface polishing quality, which defines the probability of the total internal reflection and the cutting edge effect, and the inefficient region of the bar at its edges (see Fig. 1).

A Cherenkov detector for proton Flux Measurement (CpFM) [4–6] is an in-vacuum monitor of an extracted beam halo (10-10^4 protons per bunch) with a time resolution of about $\sim$ 10 ns operating in the high radiation environment of the Super Proton Synchrotron (SPS) with a neutron flux of up to 10^{12}-10^{14} cm^{-2} year^{-1} and with an annual integrated dose tens of kGy. CpFM is conceived within UA9 experiment at CERN (see [7,8]). The quartz sensitive volume is used as Cherenkov radiation and as a light guide. This technique is also known as DIRC-Detection of Internally Reflected Cherenkov light, which is described in detail here [9–15].

In this paper, we present a report on our investigation of these effects and tests, which were performed in February 2017.

2. Experimental setup

The scheme of the experimental setup is presented in Fig. 2. It consists of two fused silica bars that are mounted parallel to the holder on the flange (non-magnetic 316NL Stainless Steel). The requested producer specifications of the bars are:

- the material is HPFC 7980 standard grade;
- all surface flat to 0.01 mm;
- all edges bevelled with a diameter of 0.1–0.2 mm;
- surface quality < 1 nm;
- typical face to side squareness < 0.02 deg;

The two bars are optically independent and they are separated from the viewport by a 2 mm thick fused silica window and are 36 mm in diameter from the PMT (Hamamatsu R7378A), powered by a high voltage supply (ISEG T2DP050205EPU 2 × 5 kV/2 mA). The PMT signal is read with USB WaveCatcher [16] electronics, which provides the rate, amplitude and charge information.

A 36.76 MBq Sr–Y radioactive source is positioned along the bars by a 3D motorised translation stage, with a position accuracy less than 100 μm. This assembly is similar to the setup installed in SPS [6]. For the given energy spectrum of the electrons, the probability to penetrate

* Corresponding author at: Taras Shevchenko National University of Kyiv (TSNUK), 60 Volodymyrska Street, City of Kyiv, 01033, Ukraine.
E-mail address: natochii@lal.in2p3.fr (A. Natochii).

https://doi.org/10.1016/j.nima.2018.08.119
Received 12 March 2018; Received in revised form 26 August 2018; Accepted 30 August 2018
Available online 8 September 2018

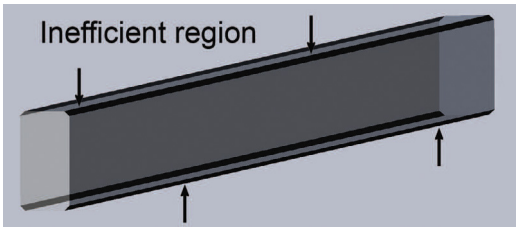

Fig. 1. Bar drawing showing the inefficient area (black arrows) in the edge of the bar which appears during the manufacturing process.

5 mm fused silica is about 10^{-5}; therefore, we can neglect the effect of the electrons crossing the two bars.

All of the components, except for the readout electronics, were placed in a "black" box that was well shielded from the outside light. Fig. 3 shows the scheme of the Sr–Y source container geometry.

Depending on the bar length, incoming angle of the electron and due to the multiple scattering inside the material [17], the photons will bounce $10 - 10^4$ times before exiting the bar. Therefore, the internal reflection coefficient must be close to one to have a good light collection at the end of the bar. For our setup the average value is about 100 reflections. The experiment investigated the dependency between the light collection on the PMT, which is aligned to be able to collect the light from both bars, and the impacting position of the electrons. The measurements were performed in steps, scanning each bar in horizontal and vertical directions separately (Fig. 4).

During the horizontal scans, due to the mechanical limitation of our setup, it was impossible to move the source up to the edge of the bar closer to the PMT, which is the origin of our reference system (Fig. 4, left). The ranges for the scan are therefore from 166 mm to 441 mm in this reference system. The translation stage was moved over 270 points with a stop of 5 s at each point.

The vertical scan was perform in the range from −20 mm to 20 mm with respect to the middle of the bar. The translation stage was moved over 40 points with a stop of 20 s at each point.

3. Experimental results

The use of USB WaveCatcher electronics provided the possibility to measure the rate (number of counts per second) of the signals from the

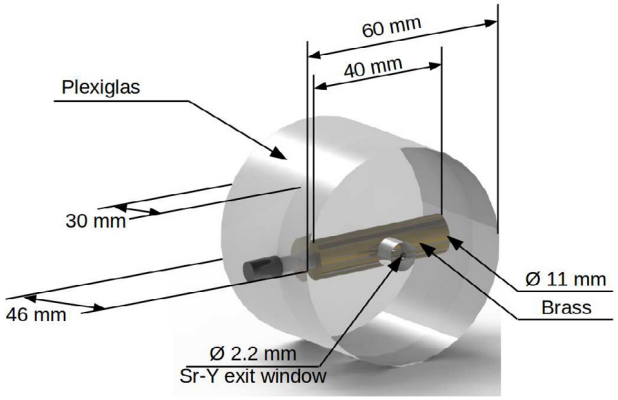

Fig. 3. Scheme of the Sr–Y source container. The source itself is located inside a brass cylinder.

PMT, which are due to the Cherenkov light produced by a β electron. Given the 36.76 MBq source activity distributed over the 4π solid angle, it is unlikely that the pile-up of the signals originated from two different electrons. The results of the measurements are illustrated in Fig. 5.

Fig. 5(a) and 5(b) show a comparison of the rate between two bars for the vertical and horizontal scans respectively. In Fig. 5(c) the data, relative to the rate for different distances between the source exit window and the surface of the bar, are reposted. To interpret the data, we fit them with the convolution function (F_{fit}) of a Gaussian and a box function (Fig. 5(d)):

$$F_{fit}(y) = (f * g)(y) \overset{\text{def}}{=} \int_{-\infty}^{\infty} f_{ab}(\tau) g(y-\tau) d\tau \Rightarrow \sum_{-20}^{20} f_{ab}(\tau) g(y-\tau) \Delta\tau \quad (1)$$

$$f_{ab}(y) = \begin{cases} 0 & \text{for } y < a. \\ 1 & \text{for } a < y < b. \\ 0 & \text{for } y > b. \end{cases} \quad (2)$$

$$g(y) = Ae^{-\frac{(y-\mu)^2}{2\sigma^2}} \quad (3)$$

where f_{ab} is the box function (a and b are the left and the right edges of the bar respectively), g is the Gaussian function with amplitude A, mean

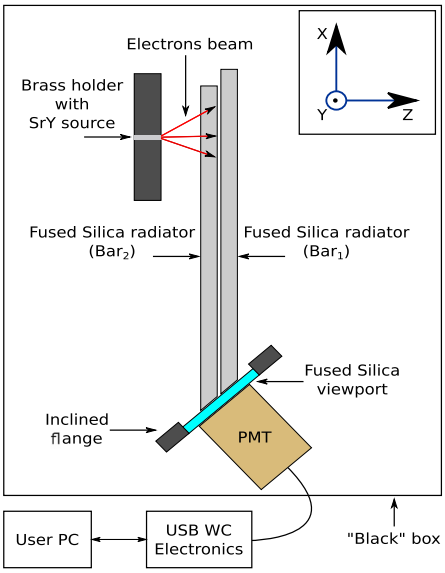

(a) Principal scheme.

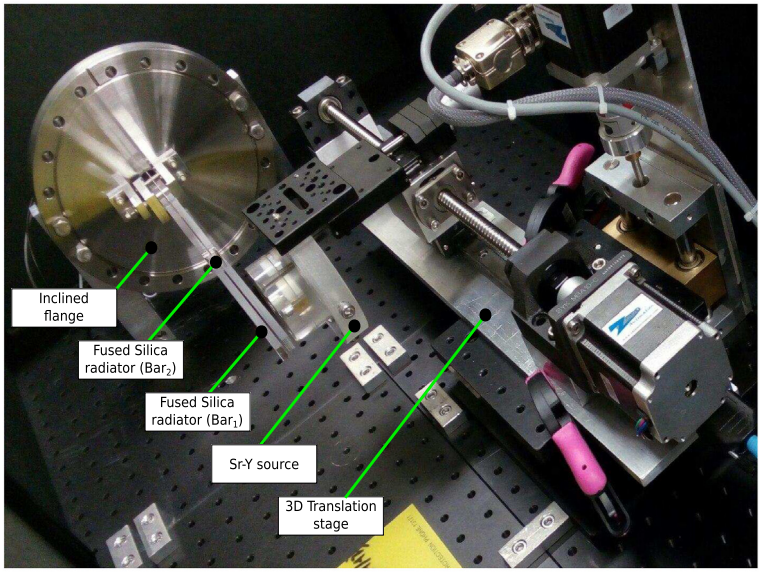

(b) Photo.

Fig. 2. Experimental setup: fused silica radiators, Sr–Y source, PMT, translation stage, readout electronics.

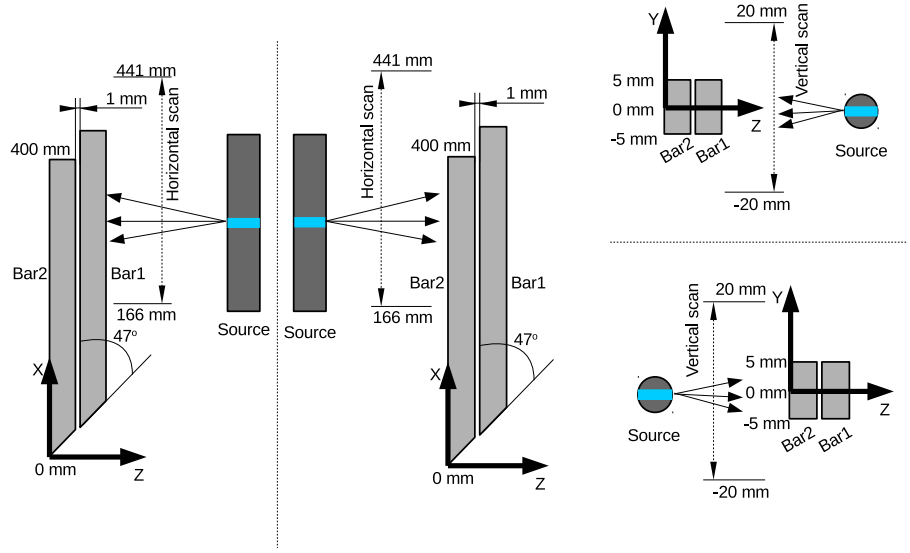

Fig. 4. Definition of the coordinate system. Horizontal and vertical scans configuration. Left: horizontal cross-section of the bar; right: vertical cross-section of the bar.

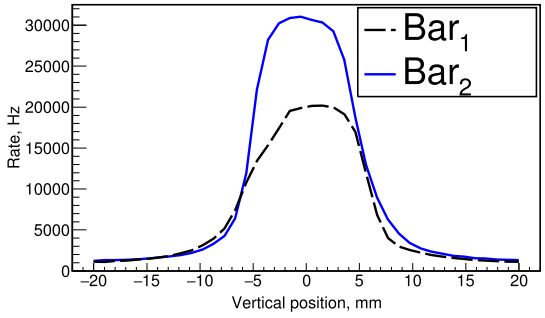

(a) Measured rates in a vertical scan for the two bars. The distance between the bar surface and the exit window of the source is 4.5 mm (along Z axis) and the horizontal position is 385 mm. The black dashed line is for Bar_1, the blue solid line is for Bar_2.

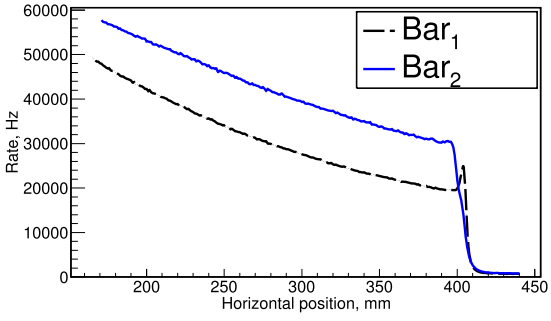

(b) Horizontal scan for two bars. Distance between bar surface and exit window of the source is 4.5 mm (in Z axis). The black dashed line is for Bar_1, the blue solid line is for Bar_2.

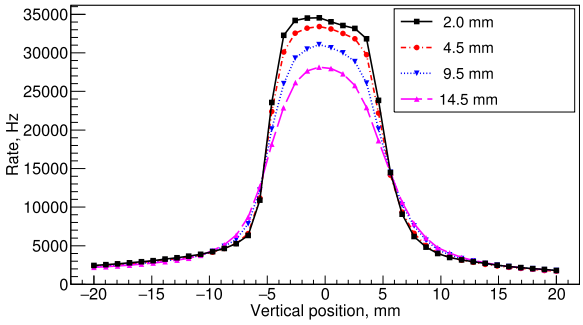

(c) Measured rates in a vertical scan for Bar_2. Different lines correspond to different distances between the bar surface and the exit window of the source (along the Z axis): black solid with squares: 2 mm, red dash-dotted with circles: 4.5 mm, blue dotted with triangles down: 9.5 mm, pink dashed with triangles up: 14.5 mm.

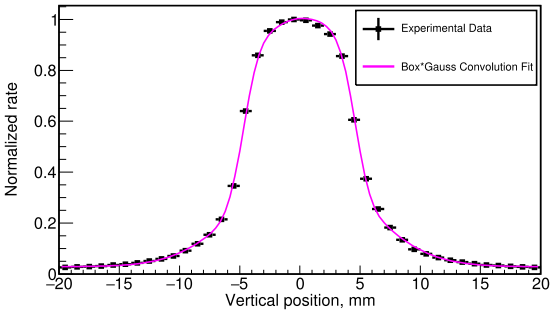

(d) Normalized (with respect to the maximum value) rate for a vertical scan (from −20 mm to 20 mm in Y axis). The data were taken for Bar_2 at 210 mm along the X axis and at a 4.5 mm distance between the bar surface and the exit window of the source (along the Z axis). The pink solid line is a fit with the convolution function (F_{fit}).

Fig. 5. Experimental results: Rate (Hz) as a function of the vertical and horizontal position of the source.

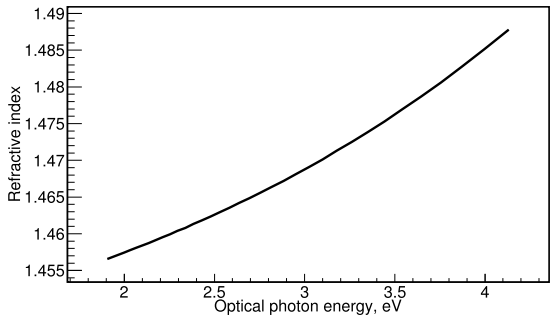

(a) Refractive index for fused silica as a function of the photon energy.

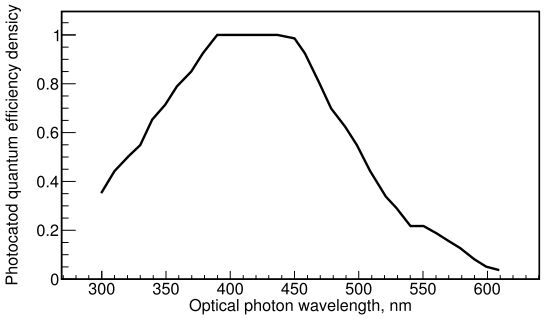

(b) Normalised Bialkali photocathode quantum efficiency as a function of the photon wavelength. Please note : 1.0 is corresponded to 24.25 %.

Fig. 6. Optical properties of the fused silica and photocathode of the PMT used in the simulation.

value μ and standard deviation σ. From the fit we derive the width of the radiator $\Delta_{ab} = 9.20 \pm 0.82$ mm and the sigma of the distribution of the particles exiting from the source $\sigma = 1.04 \pm 0.01$ mm.

4. Simulation

From Figs. 5(a) and 5(b) one can see that there is a difference in the rate between the two fused silica bars. Since the same PMT was used to readout both bars, which are geometrically identical, we can conclude that the problem comes from the mechanical or optical properties of the bars, as follows: (1) different quality of the polishing of the sides of the radiator ("polishing effect"); and (2) different quality of the edges of the radiator, leading to a different extension of the ineffective area or non-homogeneities along the bar ("edge effect").

To estimate the quality of the bar we decided to use a method based on Monte-Carlo simulation algorithms. Our goal is to reproduce the experimental data using the simulation in an iterative process. Geant4 [18] software was chosen as the framework for our modelling.

The simulation is done in two main steps, as follows:

- Realistic modelling of the β-source and validation of the distribution of the electrons using data from the vertical scan;
- Iterative simulations of the horizontal scan varying the parameters describing the quality of the bars and comparison with the experimental results to assess the correct value of the parameters.

The physical processes which were implemented in the simulation code are: particle transportation, standard EM physics, Cherenkov light production, photon interaction with matter and the ^{90}Sr radioactive decay (see Section 4.1). Other features implemented in the code are: refractive index (Fig. 6(a)) and total internal reflection probability [17] behaviour of the fused silica for different photon energies, and also quantum efficiency of the PMT Bialkali photocathode, taking into account dependence on the photon wavelength (Fig. 6(b)).

4.1. Sr–Y source

There are several possible ways to model the Sr–Y source, as follows: (1) electrons with constant energy (0.5 and 2.2 MeV of kinetic energy); (2) electrons with Sr–Y decay spectrum (using Geant4 General Particle Source); and (3) real Sr–Y decay with secondary electron and neutrinos (using Geant4 Radioactive Decay Physics). We chose the last, more comprehensive and precise method. Fig. 7 shows the β-spectrum of Sr–Y source simulated with Geant4.

Using the Geant4 radioactive decay physics, we simulated the real energy spectrum of electrons with its angular distribution.

To cross check the accuracy of our simulation of the β-source we simulated the scan in the vertical direction. In Fig. 8(a), one can see

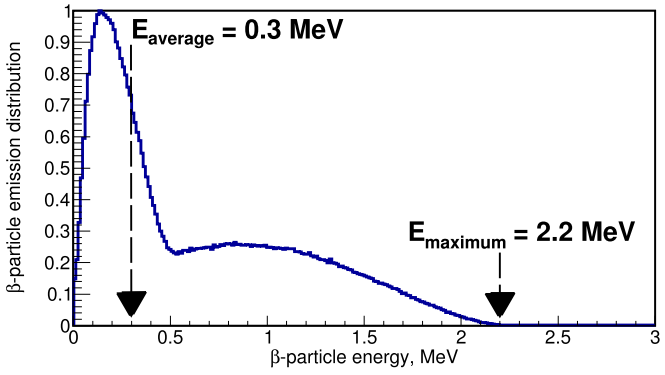

Fig. 7. The spectrum of the Sr–Y source simulated with Geant4.

a comparison of the normalised (with respect to the maximum value) rate distribution for experimental data and simulation. We fit the two distributions with the same function described previously (Eqs. (1)–(3)), adding a Gaussian and a constant term to take into account the effects due to electronics noise and light penetrating into the "lack" box. From this procedure, we get the two following main parameters: (1) $\sigma = 0.996 \pm 0.001$ mm and (2) $\Delta_{ab} = 9.3 \pm 0.8$ mm.

Fig. 8(b) shows the value of σ (which corresponds to the standard deviation of the distribution of the particles coming from the source) for different distances between the surface of the bar and the exit window of the source assembly. The value of σ linearly increases with the distance, as expected. The red curve on Fig. 8(b) confirms that the fitted width of the bar is constant for all distances. Using σ, extrapolated on the distance of 0 mm between the bar and the exit window of the source, we can estimate the dimension of the source exit window: FWHM $= 2.355 \times \sigma(0\text{ mm}) \Rightarrow$ FWHM $= 2.052 \pm 0.037$ mm, which is close enough to the real value, 2.2 mm.

This test provides an exhaustive validation of the source modelling which was a week spot of the proposed method.

4.2. Quality of the bars

To describe the quality of the bars, we defined two parameters: the probability of total internal reflection (P_{IR}) and the fraction of ineffective area at the edges of the bars (F_{IA}).

We run the simulation by performing a scan on the values of the parameters in the following ranges: $95 < P_{IR} < 100$, $0 < F_{IA} < 0.32$ and we compared simulations and experimental data using the following χ^2

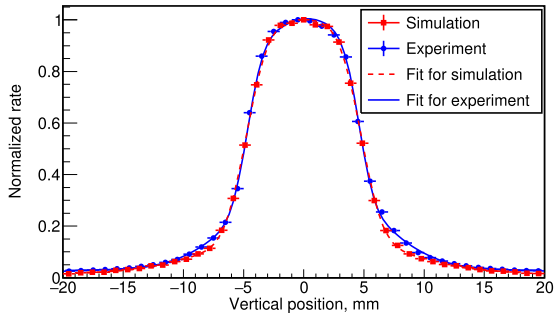

(a) Vertical scan for Bar_2: Normalized (with respect to the maximum value) rate as a function of the vertical position of the source for data and simulation with the best fit function superimposed.

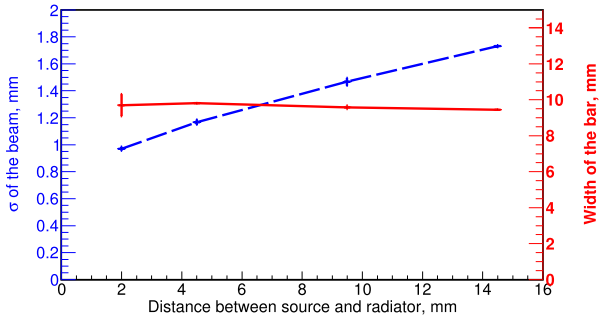

(b) The reconstructed standard deviation of a Gaussian distribution of the source particles (blue dashed curve) as a function of the distance between source and radiator (left axis); fused silica bar width (red curve) reconstructed from the fit of the experimental data as a function of the distance between source and radiator (right axis).

Fig. 8. Validation of the Sr–Y source simulation in the Geant4, measurements — data comparison. Extraction of the bar width and electron spot size from the fit.

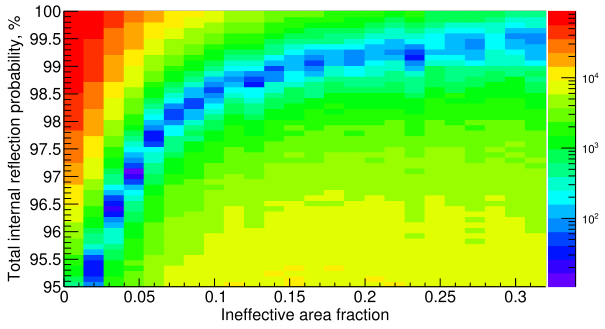

(a) χ^2 distribution of the difference between experimental and simulated data for the Bar_1.

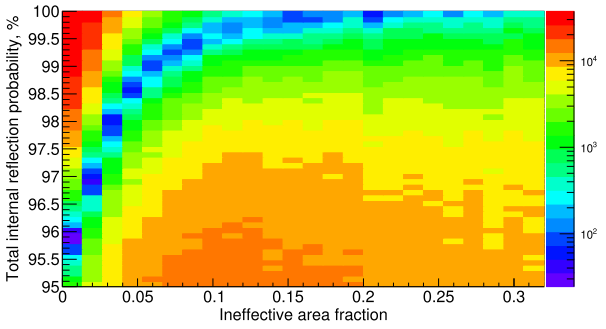

(b) χ^2 distribution of the difference between experimental and simulated data for the Bar_2.

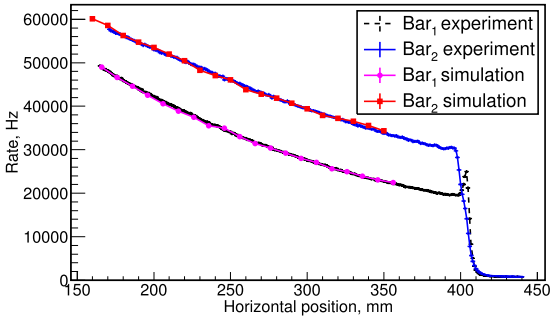

(c) Horizontal scan for Bar_1 and Bar_2. Rate (Hz) as a function of the horizontal source position, comparing between data and Geant4 simulation results. Experimental data: black dashed line is for Bar_1 and blue solid line is for Bar_2; simulation: pink solid line with circles is for Bar_1 and red solid line with squares is for Bar_2.

Fig. 9. Experimental and simulation data comparison. (For interpretation of the references to colour in this figure legend, the reader is referred to the web version of this article.)

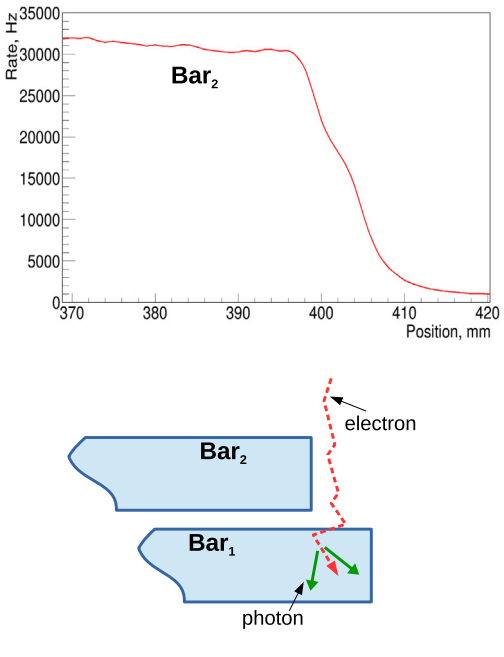

(a) Horizontal scan along Bar_2 (experimental data). Top: rate as a function of the source position; Bottom: geometrical configuration in which electrons from the source hit the Bar_1 during the scan along Bar_2. Red dashed arrows – electrons, green solid arrows – Cherenkov photons.

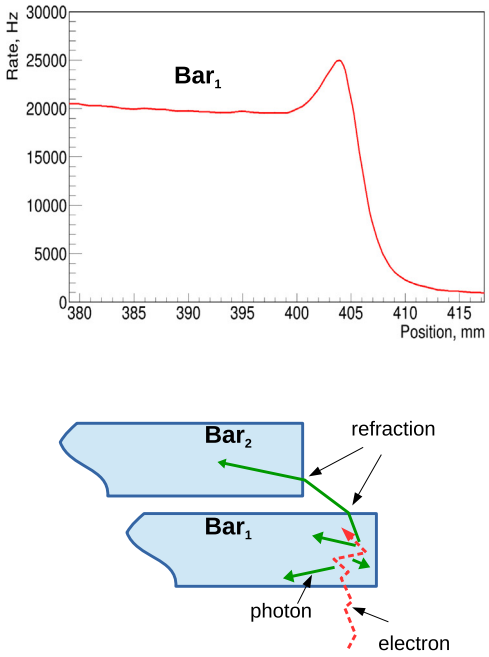

(b) Horizontal scan along Bar_1 (experimental data). Top: rate as a function of the source position; Bottom: geometrical configuration of the light crossing between bars. Red dashed arrows – electrons, green solid arrows – Cherenkov photons.

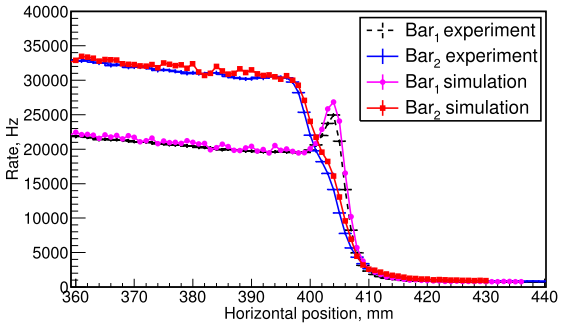

(c) Rate (Hz) as a function of the horizontal source position, comparing between data and Geant4 simulation results. Experimental data: black dashed line is for Bar_1 and blue solid line is for Bar_2; simulation: pink solid line with circles is for Bar_1 and red solid line with squares is for Bar_2.

Fig. 10. Boundary effects on the ends of the bars.

definition:

$$\chi^2 = \sum_{i=0}^{N} \left\{ \frac{(R_{exp.} - R_{sim.})^2}{(\Delta R_{exp.})^2 + (\Delta R_{sim.})^2} \right\}_i \quad (4)$$

where N is the number of measurements, which corresponds to the different positions along the bar; and, $R_{exp.}$ and $R_{sim.}$ are the normalised rate of the experimental and simulated events, respectively, with their errors $\Delta R_{exp.}$ and $\Delta R_{sim.}$. Fig. 9 shows the χ^2 for both bars as a function of the F_{IA} and the P_{IR}. We found a global minimum for Bar_1 at (F_{IA} = 2.7 ± 0.7%, P_{IR} = 96.4 ± 0.1%) and for Bar_2 at (F_{IA} = 0.0 ± 0.7%, P_{IR} = 95.9 ± 0.1%). These values correspond to the simulation results that are shown in Fig. 9(c) and well-describe the data.

The simulation of the results obtained in the horizontal scan when the source is positioned at the edge of the bars (from 400 to 410 mm in our reference system) is more difficult and should take into account the different position of the edge of the bars (Fig. 10(a)), as well as

photons that are produced in one of the bars and collected by the other (Fig. 10(b)). To take into account these boundary conditions, the χ^2 should be a function of the parameters of both bars simultaneously. Fig. 10(c) shows that our simulation describes the data remarkably well, confirming a good understanding of the process described by the simulation.

5. Conclusion

With the method described in this paper, we are able to characterise the surface quality of fused silica bars with a β-source using a simple experimental setup and a Geant4 Monte-Carlo simulation. Our model takes into account the realistic electron distribution produced by the source and it well-describes the experimental data obtained by scanning the bars with the source and measuring the Cherenkov light signal output with a PMT. In our case, we were able to estimate two parameters: the probability of total internal reflection (P_{IR}) and the fraction of ineffective area at the edges of the bars (F_{IA}) as follows: $F_{IA} = 2.7 \pm 0.7\%$, $P_{IR} = 96.4 \pm 0.1\%$ for Bar_1 and $F_{IA} = 0.0 \pm 0.7\%$, $P_{IR} = 95.9 \pm 0.1\%$ for Bar_2. The surface properties in reality are position dependent but we have assumed their small variations and estimated averaged values.

Our simulation includes the dependency between the coefficient of the total internal reflection and photon wavelength, which is received for the BaBar DIRC bars with a very good surface polishing (P_{IR} =~99.92). We assume, that the behaviour of this function is similar in our case, however, this uncertainty will contribute to the systematic error of our method.

Acknowledgments

Research was conducted in the scope of the IDEATE International Associated Laboratory (LIA).

References

[1] D. Malacara, Optical Shop Testing, third ed., John Wiley & Sons, Inc., 2007, p. 883.
[2] J. Cohen-Tanugi, et al., Optical properties of the DIRC fused silica Cherenkov radiator, Nucl. Instrum. Methods Phys. Res. A 515 (2003) 680–700, http://dx.doi.org/10.1016/j.nima.2003.07.026.
[3] G. Kalicy, et al., Status of the PANDA Barrel DIRC, J. Instrum. 9(05) (2014) C05060, http://dx.doi.org/10.1088/1748-0221/9/05/C05060.
[4] L. Burmistrov, et al., Cherenkov detector for proton flux measurement for UA9 project, in: Nuclear Science Symposium and Medical Imaging Conference (NSS/MIC), IEEE, 2013, http://dx.doi.org/10.1109/NSSMIC.2013.6829430.
[5] L. Burmistrov, et al., Test of full size Cherenkov detector for proton Flux Measurements, Nucl. Instrum. Methods Phys. Res. A 787 (2015) 173–175, http://dx.doi.org/10.1016/j.nima.2014.11.089.
[6] V. Puill, F. Addesa, L. Burmistrov, D. Breton, V. Chaumat, G. Cavoto, S. Conforti Di Lorenzo, S. Dubos, Yu.A. Gavrikov, F. Iacoangeli, J. Jeglot, J. Maalmi, A. Natochii, R. Rossi c, S. Montesano, W. Scandale a, A. Stocchi, J.-F. Vagnucci, The CpFM, an in-vacuum Cherenkov beam monitor for UA9 at SPS, J. Instrum. 12 (04) (2017) 4–29, http://dx.doi.org/10.1088/1748-0221/12/04/P04029.
[7] W. Scandale, Crystal-based collimation in modern hadron colliders, Internat. J. Modern Phys. A 25 (2010) 70–85, http://dx.doi.org/10.1142/S0217751X1004992X.
[8] W. Scandale, et al., Observation of channeling for 6500 GeV/c protons in the crystalassisted collimation setup for LHC, Phys. Lett. B 758 (2016) 129–133, http://dx.doi.org/10.1016/j.physletb.2016.05.004.
[9] B.N. Ratcliff, The B Factory Detector for PEP-II: a Status Report, SLAC-PUB-5946, 1992.
[10] B.N. Ratcliff, The DIRC counter: a new type of particle identification device for B factories, 1993, SLAC-PUB-6047.
[11] P. Coyle, et al., The DIRC counter: a new type of particle identification device for B factories, Nucl. Instrum. Methods Phys. Res. A 343 (1994) 292–299, http://dx.doi.org/10.1016/0168-9002(94)90568-1.
[12] I. Adam, et al., The DIRC particle identification system for the BABAR experiment, Nucl. Instrum. Methods Phys. Res. A 538 (2005) 281–357, http://dx.doi.org/10.1016/j.nima.2004.08.129.
[13] L. Burmistrov, The DIRC-like FTOF: A Time-of-flight Cherenkov detector for particle identification at SuperB, Acta Phys. Polon. B Proc. Suppl. 1 4 (2011) 91–99, http://dx.doi.org/10.5506/APhysPolBSupp.4.91.
[14] L. Burmistrov, N. Arnaud, D. Breton, J. Maalmi, V. Puill, A. Stocchi, D. Aston, J. Va'vra, Test of the DIRC-like TOF prototype for the SuperB experiment, Nucl. Instrum. Methods Phys. Res. A 695 (2012) 83–86, http://dx.doi.org/10.1016/j.nima.2012.01.016.
[15] N. Arnaud, et al., A particle identification detector for the forward region of the SuperB experiment, Nucl. Instrum. Methods Phys. Res. A 718 (2013) 557–559, http://dx.doi.org/10.1016/j.nima.2012.11.115.
[16] D. Breton, E. Delagnes, J. Maalmi, P. Rusquart, The WaveCatcher family of SCA-based 12-bit 3.2-GS/s fast digitizers, in: 2014 19th IEEE-NPSS Real Time Conference, 2014, pp. 1–8, http://dx.doi.org/10.1109/RTC.2014.7097545.
[17] L. Burmistrov, A Detector for Charged Particle Identification in the Forward Region of SuperB (Ph.D. thesis), 2011, pp. 1–234, LAL 11-299, http://www.theses.fr/2011PA112331.pdf.
[18] J. Allison, et al., Recent developments in Geant4, Nucl. Instrum. Methods Phys. Res. A 835 (2016) 186–225, http://dx.doi.org/10.1016/j.nima.2016.06.125.